

Accepted Manuscript

Synthesis, mesomorphic properties and nonlinear optical studies of alkyl and alkoxy phenylacetylene containing phenazine fused extended triphenylene discotic liquid crystalline dyes

Ashwathanarayana Gowda, Litwin Jacob, Alakananda Patra, Agnes George, Reji Philip, Sandeep Kumar

PII: S0143-7208(18)31383-4

DOI: [10.1016/j.dyepig.2018.07.052](https://doi.org/10.1016/j.dyepig.2018.07.052)

Reference: DYPI 6906

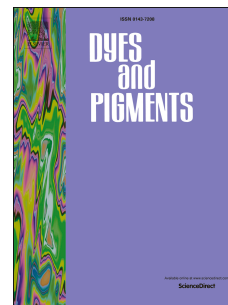
To appear in: *Dyes and Pigments*

Received Date: 21 June 2018

Accepted Date: 28 July 2018

Please cite this article as: Gowda A, Jacob L, Patra A, George A, Philip R, Kumar S, Synthesis, mesomorphic properties and nonlinear optical studies of alkyl and alkoxy phenylacetylene containing phenazine fused extended triphenylene discotic liquid crystalline dyes, *Dyes and Pigments* (2018), doi: 10.1016/j.dyepig.2018.07.052.

This is a PDF file of an unedited manuscript that has been accepted for publication. As a service to our customers we are providing this early version of the manuscript. The manuscript will undergo copyediting, typesetting, and review of the resulting proof before it is published in its final form. Please note that during the production process errors may be discovered which could affect the content, and all legal disclaimers that apply to the journal pertain.



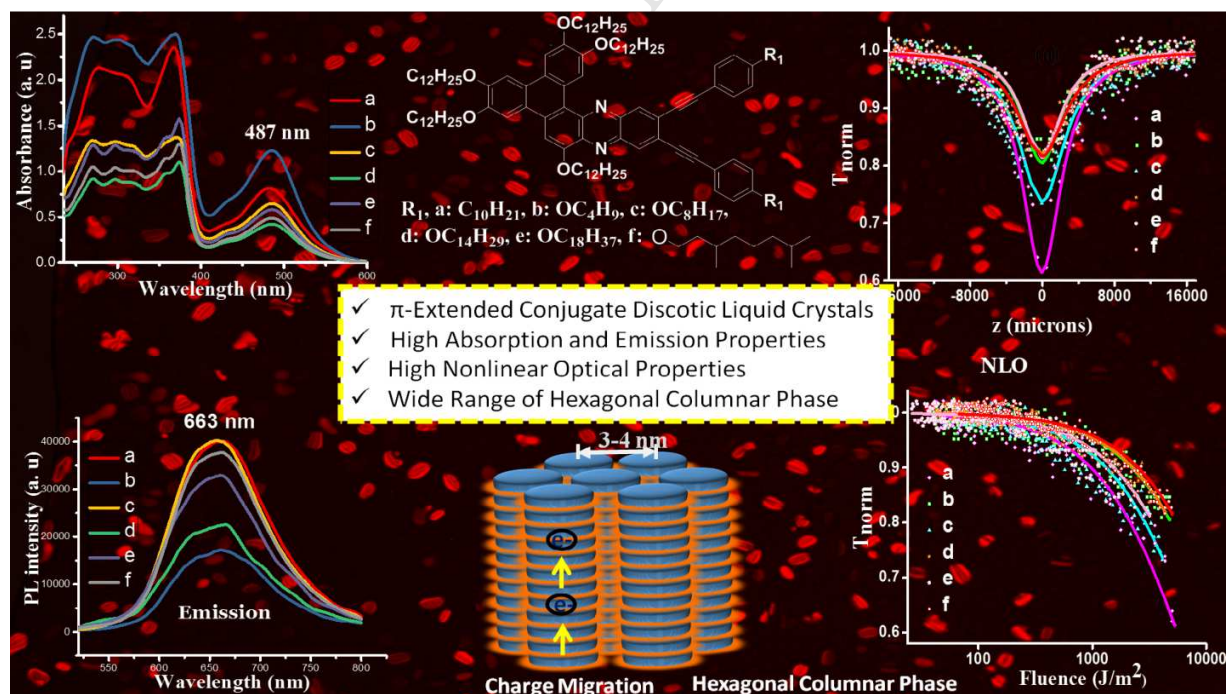
Graphical abstract:

Synthesis, mesomorphic properties and nonlinear optical studies of alkyl and alkoxy phenylacetylene containing phenazine fused extended triphenylene discotic liquid crystalline dyes

Ashwathanarayana Gowda, Litwin Jacob, Alakananda Patra, Agnes George, Reji Philip and Sandeep Kumar *

Raman Research Institute, C.V. Raman Avenue, Sadashivanagar, Bangalore - 560 080, India

Phone: +91 80 23610122, Fax: +91 80 23610492, E-mail: skumar@rri.res.in



Synthesis, mesomorphic properties and nonlinear optical studies of alkyl and alkoxy phenylacetylene containing phenazine fused extended triphenylene discotic liquid crystalline dyes

Ashwathanarayana Gowda, Litwin Jacob, Alakananda Patra, Agnes George, Reji Philip and Sandeep Kumar *

Raman Research Institute, C.V. Raman Avenue, Sadashivanagar, Bangalore - 560 080, India

Phone: +91 80 23610122, Fax: +91 80 23610492, E-mail: skumar@rri.res.in

Abstract:

Herein, we have reported the alkyl and alkoxy phenylacetylene containing phenazine fused triphenylene discotic liquid crystals (DLCs) which are obtained by the condensation reaction of triphenylene-1,2-diquinone with 1,2-diamino-4,5-dibromobenzene, followed by Sonogashira C–C coupling reaction with 4-alkyl-phenylacetylene or 4-alkoxy-phenylacetylene. Six novel derivatives were synthesized and evaluated for their thermal and optical properties. They show a broad range of hexagonal columnar phase and retain their mesophase up to room temperature upon cooling from the isotropic liquid. Thermotropic liquid crystalline properties of all the compounds were studied by polarized optical microscopy (POM), differential scanning calorimetry (DSC). The self-assembly of mesophase structure was investigated by X-ray diffraction (XRD) studies. Thermogravimetric analysis of all the mesogens shows good thermal stability over a broad temperature range. The photophysical properties of newly synthesized compounds were measured using UV-Vis absorption and photoluminescence emission spectroscopy in anhydrous chloroform solvent. The π -extended conjugation in these mesogens

exhibit strong absorption bands falling around 270–487 nm and corresponding emission band at 657–663 nm respectively. The high delocalization of π - electrons in extended discotic mesogens show high nonlinear optical properties when measured under excitation by nanosecond laser pulses at 532 nm. These materials may find distinctive applications in the semiconducting devices.

Keywords: Discotic liquid crystals, triphenylene, Sonogashira coupling, columnar phase, nonlinear optical transmission.

1. Introduction

The spontaneous self-assembly of nanostructured materials generated by utilizing non-covalent interactions such as van der Waals forces, π - π interactions, H-bonding, charge transfer, ionic interactions, dipolar and quadrupolar interactions and so on are extremely important in the soft material science [1–4]. Liquid crystals (LCs) belong to this family of self-assembled supramolecular architectures which can be used as potential anisotropic materials for commercial applications [5]. The discovery of discotic liquid crystals (DLCs) obtained from disc-shape molecules by S. Chandrasekhar, et al. in 1977, opens scientific evolution in the soft material science [6–10]. The appropriate functionalization of disc-shape molecules leads to the formation of DLCs via self-organization and self-assembly. The self-healing and self aligning ability of DLCs are remarkable properties responsible for forming highly ordered supramolecular architectures which have been recognized as molecular wires in various electronic device applications [11–17]. Most of the DLCs are derived from polycyclic aromatic cores such triphenylene (TP), anthraquinone (AQ), phthalocyanine (Pc), hexabenzocoronene (HBC) and so

on, surrounded by a mantle of flexible aliphatic chains [7,18–22]. Orientational order of discs forms the nematic phase which has found commercial applications as optical compensating films in wide viewing LCDs [9,19,22–26]. The strong π - π interactions between aromatic cores favour columnar stacking of the molecules, where individual molecules stacked one on top of the other to form columns. The high charge carrier mobility in DLCs arises due to the stacking arrangement of discs which provides facile π -electrons overlap in only one direction. The electrons or hole migrates effectively along the columns in quasi one dimension [11–16]. Eventually, the electrical conductivity along the columns have been observed several orders of magnitude greater than that in perpendicular direction [27–36]. Hence, due to this peculiar behavior, DLCs have been extensively applied in organic light emitting diodes (OLEDs), [37–39], organic field effect transistors (OEFT) [40–42], photovoltaic solar cells [11,43,44] and sensors [45,46] etc.

Triphenylene is the most widely studied discotic core. The appropriate chemical modification of triphenylene (TP) is known to exhibit various stable columnar mesophases [7,47–51]. The nature of alkyl chains and functional groups substitutions on TP core show stable mesophases over broad temperature range having interesting electronic properties. The electron rich nature of TP derivatives makes them suitable for doping with electron acceptors to gives *p*-type of organic semiconductors. Extension of TP discotic core significantly changes the liquid crystalline behaviour and electronic properties. Such macromolecular macro discs exhibit wide range of mesophase and high charge carrier mobility in the columnar phases [52,53]. Many synthetic methods have been employed to extend the triphenylene core to produce phenanthrophenazine [54,55], hexabenzotriphenylene [56], triphenylenophthalocyanine [57], etc. Cammidge et al. reported TP discotic twins fused via pyrazine heteroaromatic ring and they exhibit stable

hexagonal columnar phase over broad temperature range [58]. Wu et al. synthesised triphenylene-fused triazatruxenes based π -extended discotic liquid crystals and investigated their charge carrier mobility and gelation properties. The higher homologues in the series exhibit high hole mobility (*p*-type) of $0.8 \text{ cm}^2 \text{ V}^{-1} \text{ s}^{-1}$ [59]. We have reported synthesis and liquid crystalline properties of imidazole fused triphenylene discotic liquid crystals [60]. Very recently, we have also investigated the charge carrier mobility of phenazine fused triphenylene discotic liquid crystals containing alkanethiols and alkoxy chains. We have observed that hole mobility of the order of $10^{-4} \text{ cm}^2 \text{ V}^{-1} \text{ s}^{-1}$ in its hexagonal columnar mesophase [61].

In the present investigation, we have synthesised symmetrical phenazine-fused-triphenylene derivatives to look the effect of extension of discotic core on the liquid crystalline properties. Here, we report alkyl and alkoxy phenylacetylene containing phenazine fused triphenylene DLCs with enhanced π -electron conjugation. We designed and synthesized extended triphenylene DLCs as shown in Scheme 1. We discuss the synthesis, characterisation and mesomorphic properties of novel extended phenazine fused triphenylene derivatives. All the novel compounds were characterised using spectral and elemental analysis. The liquid crystalline behaviour of all the compounds was investigated by polarised optical microscopy (POM) and differential scanning calorimetry (DSC). The mesophase structure of all the mesogens were investigated using X-ray diffraction studies (XRD). Further, the photophysical and nonlinear optical studies were also investigated for all the mesogens (**14a–14f**).

2. Results and Discussions

2.1. Synthesis

The synthesis of π -extended phenazine fused triphenylene discotic liquid crystals is shown in **Scheme 1**. The intermediate monohydroxytriphenylene **11** was prepared following reported procedure starting from catechol [62]. Its oxidation with ceric ammonium nitrate (CAN) produces 3,6,7,10,11-pentakis(dodecyloxy)triphenylene-1,2-diones **12** [63]. The another intermediate compound 4,5-dibromobenzene-1,2-diamine **4** was synthesized using a reported procedure [64]. Its condensed with triphenylene-1,2-diquinone in presence of glacial acetic acid gives 13,14-dibromo-2,3,6,7,10-pentakis(dodecyloxy)phenanthro[9,10-a]phenazine discotic mesogen **13** [61]. Sonogashira C–C bond coupling reaction of 4-alkyl phenylacetylene or 4-alkoxy phenylacetylene **8** [65] with mesogenic compound **13** in the presence of bis(triphenylphosphine)palladium(II) dichloride ($\text{PdCl}_2(\text{PPh}_3)_2$) and copper(I) iodide (CuI) in anhydrous triethylamine (TEA) solvent offered final discotic liquid crystal compounds (**14a–14f**). From UV absorption spectra, it is clearly indicated that the appearance of new red shifted peak at 487 nm is obtained from the π -extension of triphenylene ring.

2.2. Mesomorphic properties

The thermotropic liquid crystalline behaviour of all the synthesised compounds (**14a–14f**) was first viewed using optical microscopy with crossed polarisers which display characteristic defect texture of columnar phase. The exact phase transition temperature (peak temperature in °C) and associated enthalpy values (ΔH in kJ mol^{-1}) were investigated with the help of DSC measurement on both heating and subsequent cooling scans with a scan rate of 10 °C min^{-1} and recorded under nitrogen atmosphere. The phase transition temperature of all mesogens agrees very well with POM observations, as summarized in Table 1.

Table 1. Phase behaviour of discotic mesogens (**14a–14f**).

Cr = crystalline phase; Col_h = hexagonal columnar phase; I = isotropic phase.

Compound	Phase transition peak temperature (°C); (ΔH , [kJ mol^{-1}])	
	Second heating scan	Second cooling scan
14a	Cr 37.2 [44.0] Col _h 217 [3.2] I	I 209.3 [-3.1] Col _h 12.2 [-38.3] Cr
14b	Cr 64.8 [50.0] Col _h 231.7 [2.1] I	I 224.4 [-2.2] Col _h 27.3 [-39.5] Cr
14c	Cr 49.9 [42.9] Col _h 228.5 [4.0] I	I 221.7 [-2.5] Col _h 21.2 [-41.1] Cr
14d	Cr 49.0 [39.5] Col _h 163.6 [2.3] I	I 162.2 [-2.2] Col _h 23.3 [-42.7] Cr
14e	Cr 69.5 [79.1] Col _h 139.4 [0.6] I	I 135.1 [-0.7] Col _h 37.1 [-71.6] Cr
14f	Cr 40.9 [45.3] Col _h 200.3 [2.7] I	I 196.9 [-2.6] Col _h 19.6 [-41.9] Cr

All the mesogens exhibit wide range of enantiotropic hexagonal columnar mesophase with two types of endothermic phase transition from crystal to Col_h at lower temperature and Col_h phase to isotropic phase at higher temperature and they retain columnar phase up to room temperature upon cooling from the isotropic liquid. The first compound in the series **14a**, with mixed alkyl and alkoxy chains, melts at 37.2 °C with phase transition enthalpy 44 kJ mol⁻¹ to Col_h phase and transition from Col_h phase to isotropic phase at 217 °C ($\Delta H = 3.2$ kJ mol⁻¹). Upon slow cooling from the isotropic liquid under POM, the texture with rectilinear defects of Col_h phase was observed as shown in Fig. 1a. As a representative example of DSC thermogram of compound **14a** is shown in Fig. 2. The compound **14b** with alkoxy chains melts to Col_h at 64.8 °C ($\Delta H = 50$ kJ mol⁻¹) and Col_h to isotropic liquid at 231.7 °C with corresponding heat transition ($\Delta H = 2.1$ kJ mol⁻¹) (ESI, Fig. S2). Columnar textures were observed upon cooling from the isotropic liquid at 224.4 °C (ESI, Fig. S1). On the other hand, compounds **14c** and **14d** exhibit phase transition from crystalline phase to columnar phase at 49.9 °C ($\Delta H = 42.9$ kJ mol⁻¹) and 49 °C ($\Delta H = 39.5$ kJ mol⁻¹) respectively, and the peak temperatures at 228.5 °C ($\Delta H = 4.0$ kJ mol⁻¹) and 163.6 °C ($\Delta H = 2.3$ kJ mol⁻¹) were attributed to Col_h to isotropic phase transition (ESI, Fig. S1 & S2). Under POM, the compound **14c** exhibit mesophase texture at 221.7 °C (on cooling) as shown in Fig. 1b. The compounds **14d** exhibit similar mesophase texture observed under POM upon cooling from isotropic liquid (ESI, Fig. S1). Similarly, compound **14e** transformed to Col_h phase at 69.5 °C ($\Delta H = 79.1$ kJ mol⁻¹) at lower temperature and Col_h to isotropic phase at 139.4 °C ($\Delta H = 0.6$ kJ mol⁻¹) at higher temperature (Fig. S2). The compound **14f** with branched alkoxy chain show similar behaviour, peak temperature at 40.9 °C, with enthalpy change at 45.3 kJ mol⁻¹ characteristic for Cr to Col_h phase and Col_h to isotropic liquid at 200.3 °C ($\Delta H = 2.7$ kJ mol⁻¹).

(Fig. S2). Upon cooling under POM, the mesophase texture appeared at 135.1 °C (**14e**) and 196.9 °C (**14f**) respectively (ESI, Fig. S1).

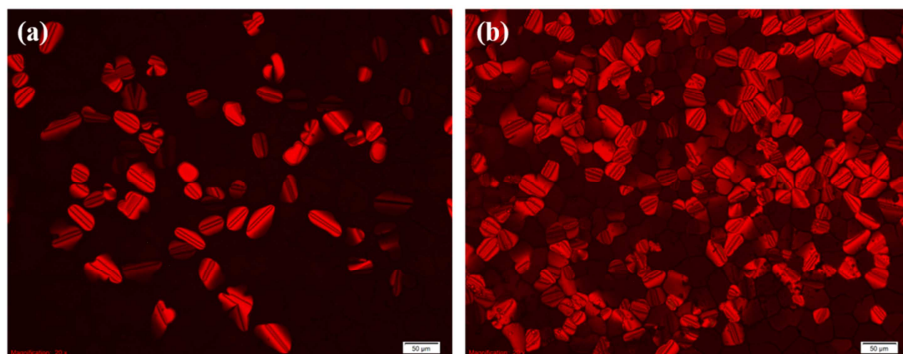


Fig. 1. Polarised optical microscopy textures for compound **14a**, (a) early growing rectilinear defect texture of Col_h phase at 202 °C, viewed at 100 \times magnification; for compound **14c** (b) hexagonal columnar texture recorded at 114 °C, viewed at 200 \times magnification. Both POM images were recorded on slow cooling from the isotropic liquid.

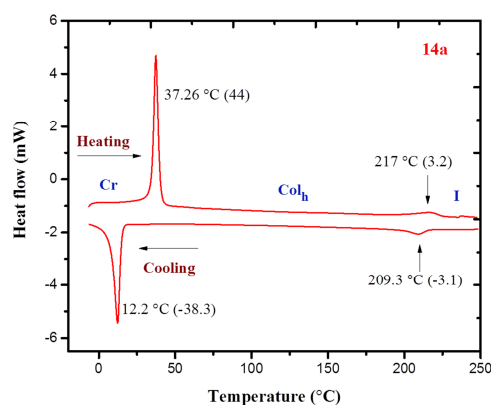


Fig. 2. DSC thermogram of compound **14a** showing phase transitions on heating and cooling cycles at a scan rate of 10 °C min⁻¹. Vertical arrows indicate phase transition points.

Thermal stability of all the discotic mesogens (**14a–14f**) was measured using thermogravimetric analysis (TGA). All the compounds were subjected to heat scan of $10\text{ }^{\circ}\text{C min}^{-1}$ under a nitrogen atmosphere. All the compounds were found stable up to $365\text{--}375\text{ }^{\circ}\text{C}$ depending on the alkyl chain length as shown in Fig. S3. All the compounds initiated weight loss at $385\text{ }^{\circ}\text{C}\text{--}400\text{ }^{\circ}\text{C}$ and decomposed at $480\text{ }^{\circ}\text{C}$. The decomposition temperature of the mesogens was much higher than the isotropic temperature. It inferred that all the compounds possess good thermal stability over broad temperature.

3. X-ray diffraction measurements

In order to understand the mesophase structure of all the novel mesogens, X-ray diffraction experiments were carried out using LC samples filled in Lindemann capillaries. X-ray diffraction patterns are recorded for all the mesogens (**14a–14f**) in the hexagonal columnar mesophase on both heating and subsequent cooling scans as shown in Table 2 and a representative example is shown in Fig. 3. All the mesogenic compounds **14a–14f** showed increasing order of diffraction angle. The d -spacing of the first reflection in the small angle region to the second one is in the ratio of $1:1/\sqrt{3}:1/2:1/\sqrt{7}$. These values corresponding to those obtained from two-dimensional hexagonal lattice and relatively broad peaks in the wide angle regime corresponding to the liquid like packing of the molten aliphatic chains and core-core separation. The intercolumnar distance, a , calculated by using the relation $a = d_{10}/(\cos 30^{\circ})$, where d_{10} is the spacing corresponding to the strongest peak in the small angle region (Table 2). As a representative and typical XRD pattern obtained for compound **14a** (on heating scan) and **14d** (on cooling scan) are shown in Fig. 3. The XRD pattern of compound **14a** at $100\text{ }^{\circ}\text{C}$ on heating in the columnar phase is shown in Fig. 3a and respective lattice parameters were tabulated in Table 2. In the small angle region four peaks being observed, one very strong and other three weak peaks of d -spacing $d_1 = 28.26\text{ \AA}$, $d_2 =$

16.24 Å, $d_3 = 14.07$ Å and $d_4 = 10.64$ Å respectively, values are in agreement with the hexagonal columnar lattice. The broad peak at wide angle region $d = 4.65$ Å corresponds to liquid like packing of molten aliphatic chains and the intercolumnar distance is found to be 32.63 Å respectively (Fig. 3a). Similarly, X-ray diffraction pattern obtained for compound **14d** in the columnar phase at 70 °C on cooling from the isotropic liquid is shown in Fig. 3b. The compound **14d** shows similar reflections in the small angle regime with d -spacing $d_1 = 30.04$ Å, $d_2 = 17.24$ Å and $d_3 = 14.95$ Å. The broad peak in wide angle regime at 4.66 Å corresponds to a flexible alkyl chain length and the core-core gap is 3.54 Å. It is evident that with an increase in the number of alkyl chain length, the width of the columns obtained discotic molecules also increases. Similar X-ray diffraction patterns were obtained for all other compounds as shown in Fig. S4. The above results further confirmed that all the mesogenic derivatives are self-assembled in the hexagonal columnar fashion in their liquid crystal phase as shown in graphical model Fig. 4.

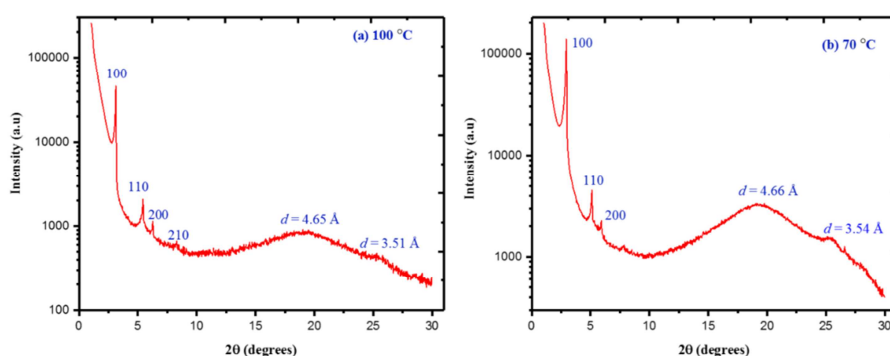


Fig. 3. The intensity profile of the X-ray pattern: (a) **14a** at 100 °C (heating scan) and (b) **14d** at 70 °C (cooling scan) respectively.

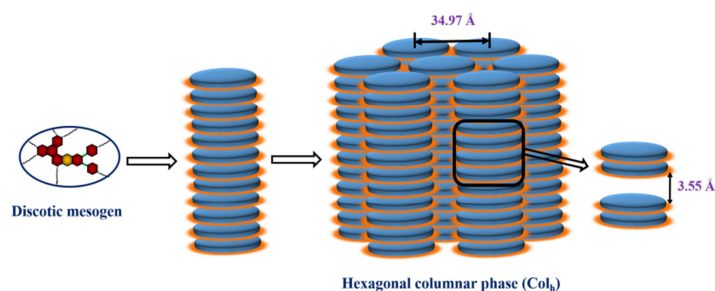


Fig. 4. Schematic representation of self-assembly of hexagonal columnar phase obtained for the representative compound **14e**.

Table 2. XRD data of all the discotic mesogens (**14a-14f**)

Compound	Temperature (°C)	2θ (degrees)	d -Spacings (Å)	Col_h Parameters	Miller indices	Alkyl-chain length (Å)	Core-Core separation (Å)	Intercolumnar distance (a) (Å)
14a	100	3.12	28.26	1	100	4.65	3.51	32.63
		5.43	16.24	$1/\sqrt{3}$	110			
		6.273	14.07	$1/2$	200			
		8.29	10.64	$1/\sqrt{7}$	210			
14b	122	3.56	24.73	1	100	4.50	3.61	28.67
		6.19	14.25	$1/\sqrt{3}$	110			
		7.14	12.36	$1/2$	200			
14c	70	3.25	27.12	1	100	4.49	3.52	31.40
		5.61	15.71	$1/\sqrt{3}$	110			
		6.50	13.51	$1/2$	200			
14d	70	2.93	30.04	1	100	4.66	3.54	34.68
		5.11	17.24	$1/\sqrt{3}$	110			
		5.90	14.95	$1/2$	200			
14e	85	2.91	30.23	1	100	4.62	3.55	34.97
		5.03	17.51	$1/\sqrt{3}$	110			
		5.80	15.24	$1/2$	200			
14f	65	3.12	28.28	1	100	4.60	3.48	32.65
		5.43	16.25	$1/\sqrt{3}$	110			
		6.24	14.13	$1/2$	200			
		8.26	10.65	$1/\sqrt{7}$	210			

4. Photophysical properties

The photophysical properties of all the novel discotic mesogens were investigated by a Perkin-Elmer UV-Vis lambda 35 double-beam spectrometer and photoluminescence (PL) spectra using spectrofluorometer (Fluorolog-3, Horiba Jobin Yvon). The UV-absorption properties of all the liquid crystalline compounds (**14a–14f**) were studied in anhydrous chloroform solvent (10^{-5} M) recorded at room temperature to determine absorption maxima as presented in Fig. 5 (a) and the respective absorption values are summarized in Table 3. Compound **14a** having 4-alkyl phenylacetylene chains show maximum absorption (λ_{\max}) bands at 482 nm and 368 nm which corresponds to $n-\pi^*$ and $\pi-\pi^*$ transitions of triphenylene ring containing extended 4-alkyl-phenylacetylene fused phenazine derivative. The less intense peaks at 313 nm, 217nm may be because of $\pi-\pi^*$ transitions of aromatic benzene rings. The alkoxy chain compounds **14b–14f** exhibit similar kind of absorption behaviour with λ_{\max} corresponds to $n-\pi^*$ transitions at 485–487 nm and $\pi-\pi^*$ transition at 374 nm along with negligible shoulder peak around 360 nm. Compounds **14d**, **14e** and **14f** with longer alkyl chain length show λ_{\max} corresponds to $n-\pi^*$ transitions at 485–487 nm and $\pi-\pi^*$ transition at 370–374 nm along with negligible shoulder peak around 360 nm. The less intense peaks at around 297 nm and 270 nm correspond to $\pi-\pi^*$ transitions of benzene ring. The high delocalized electronic system and high molar absorption coefficients ($\epsilon = 4.6-5.8 \times 10^6 \text{ L mol}^{-1} \text{ cm}^{-1}$) attribute to the maximum absorption in this novel mesogens. In general, the maximum light absorption depends on the molecules that absorb light of a given wavelength. It is also known that extended delocalised π -electron conjugation present in these discotic mesogens causes bathochromic shift (longer wavelength).

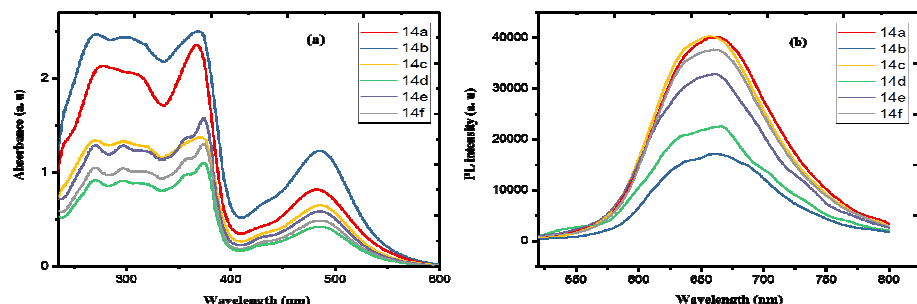


Fig. 5. (a) UV-Visible absorption spectra and (b) fluorescence emission spectra of all the discotic mesogens (**14a–14f**).

Photoluminescence spectra of all the mesogens (**14a–14f**) were recorded in anhydrous chloroform solvent. The emission spectra were recorded using a slit size of 2 nm in dilute anhydrous chloroform solution at room temperature and all the compounds were excited at $\lambda_{\max} = 490$ nm. All the mesogens exhibit strong emission band at 657–663 nm. A Stokes shift in the range of 286–295 nm was observed for all the mesogens (Table 3).

Table 3. Photophysical properties of discotic mesogens recorded using anhydrous chloroform (10^{-5} M).

Compound	Absorption $\lambda_{\text{abs}}/\text{nm}$ ($\epsilon/10^6 \text{ L mol}^{-1} \text{ cm}^{-1}$)	Emission/ nm
14a	277, 313, 368, 482 (5.3)	663
14b	270, 300, 370, 485 (4.6)	661
14c	270, 296, 371, 486 (5.7)	657
14d	270, 297, 360, 374, 486 (5.8)	663
14e	270, 297, 360, 374, 487 (5.7)	660

14f	271, 297, 359, 374, 485 (5.3)	660
------------	-------------------------------	-----

5. Nonlinear optical studies

Nonlinear optical studies of all the discotic mesogens (**14a–14f**) are carried out by utilizing the open aperture Z-scan technique using a frequency doubled Nd:YAG laser (Minilite I, Continuum) providing linearly polarized Gaussian of 5 ns pulse width at 532 nm wavelength. The experimental setup consists of the laser source, focusing lens, a 1 mm quartz cuvette containing sample (which is fixed on a stepper motor controlled translation stage) and a pyroelectric detector (Fig. S5).

The laser light is focused using a lens of focal length 9.5 cm along the z axis. All the discotic mesogens (**14a–14f**) were dissolved in anhydrous chloroform solvent, which is kept between the focusing lens and the detector and moved along the z axis, in order to change the laser fluence. The transmitted energy is then measured using the pyroelectric detector (Laser probe, RJP-735). The open aperture Z-scans obtained are shown in Fig.6.

The fluence of the laser beam, which is a function of position with respect to the focal point, is given by

$$F_{in}(z) = 4(\ln 2)^{\frac{1}{2}} E_{in} / \pi^{\frac{3}{2}} \omega(z)^2 \dots \dots \dots (1)$$

Where E_{in} is input energy (3 μ J) and $\omega(z) = \omega_0 \left(1 + \left(\frac{z}{z_0}\right)^2\right)^{\frac{1}{2}}$, ω_0 is the radius of the laser beam at the focus, and z_0 is the Rayleigh length given by $z_0 = \pi \omega_0^2 / \lambda$.

The normalized transmittance (T_{norm}) vs. position graph is plotted to obtain the Z-scan curve. The pulse propagation equation is given by

$$\frac{dI}{dx} = - \left[\frac{\alpha_0}{1+I/I_s} + \beta I \right] I \dots\dots\dots (2)$$

With $\alpha(I)$ being the net nonlinear absorption coefficient,

$$\alpha(I) = \frac{\alpha_0}{1+I/I_s} + \beta I \dots\dots\dots (3)$$

where I_s is the saturation intensity (in W/m^2) and β is the reverse saturable absorption coefficient (in m/W). These parameters can be obtained by numerically fitting the measured nonlinear transmission data to equation 2.

The calculated values of I_s and β are given in Table 1. While doing the numerical calculations, we noticed that though RSA [66,67] dominates the nonlinearity, SA [68], which is not very obvious from the measured Z-scan curves, is also present in the system and should be accounted by including, I_s in the calculation for getting good fits. The high NLO response of discotic mesogens arises due extended conjugation. The donor ability of symmetrical π -extended phenylacetylene groups through alkyne spacer and heteroaromatic phenazine acceptor ring enhance the intramolecular delocalization of π -electrons, which are responsible for high nonlinear properties in these materials. These high NLO materials are subject of numerous investigations of photonic applications like optical switches and optical limiters etc. [69]

Table 4: β and I_s values calculated for the samples

Compounds	Linear transmittance	β $\times 10^{-11} m/W$	I_s $\times 10^{11} W/m^2$
14a	0.57	96	25

14b	0.69	36	50
14c	0.57	72	32
14d	0.69	41	28
14e	0.62	61	55
14f	0.69	34	45

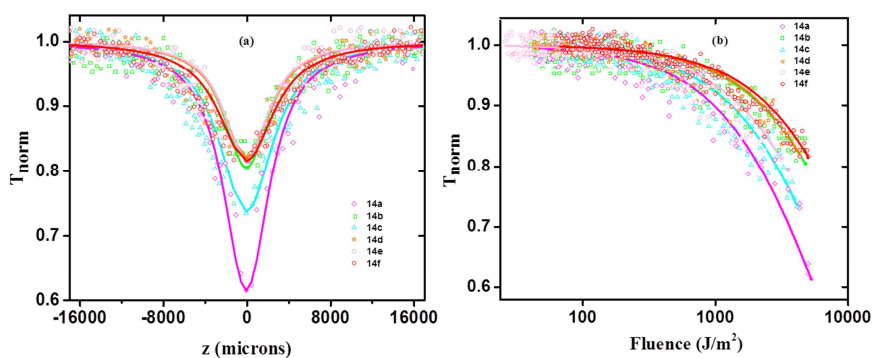


Fig. 6. (a) Open aperture Z-scan measurements done at the laser pulse energy of 3 micro Joules, (b) Normalized transmission as a function of input laser fluence, calculated from the Z-scan data.

6. Experimental section

6.1. General procedure for the synthesis of final compounds

The compounds 4,5-dibromobenzene-1,2-diamine **4** [55], 1-ethynyl-4-alkoxybenzene **8** [56], 3,6,7,10,11-pentakis(alkyloxy)triphenylene-1,2-diones **8** [54], and 13,14-dibromo-2,3,6,7,10-pentapropoxyphenanthro[9,10-a]phenazine [52] were synthesized as reported and confirmed by spectral and elemental analysis.

Synthesis of 13,14-bis(2-(4-decylphenyl)ethynyl)-2,3,6,7,10-pentakis(dodecyloxy) phenanthro[9,10-a]phenazine (14a) and 13,14-bis(2-(4-alkoxyphenyl)ethynyl)-2,3,6,7,10-penta(alkoxy)phenanthro[9,10-a]phenazine (14b–14f).

To a stirring solution of compound **13** (0.5 g, 1 eq.) in triethylamine (40 mL) solvent was added PdCl₂(PPh₃)₂ (0.06 eq.) and CuI (0.07 eq.) under argon atmosphere. The resulting reaction mixture was allowed to stirred for 10 mines under argon at room temperature. To this, 1-decyl-4-ethynylbenzene or 1-ethynyl-4-alkoxybenzene (2.6 eq.) was added under argon flow. The resulting reaction mixture was heated to 72 °C for 24 h. After completion of reaction, the reaction mixture was allowed to cool to room temperature and diluted with diethyl ether, followed by filtered through celite pad. The filtrate was washed with excess of water and extracted with diethyl ether (3 × 40 mL). The combined extracts were dried over Na₂SO₄ and solvent was evaporated under vacuum. The residue was purified by column chromatography using silica gel (*n*-hexane/dichloromethane 9:1). Recrystallisation of the pure product with absolute ethanol affords dark red color solid (**14a–14f**) in about 65–70% yield.

14a: IR (film) ν_{\max} = 2951, 2922, 2852, 2216, 1624, 1516, 1456, 1375, 1261, 1163, 1080 cm⁻¹; ¹H NMR (500 MHz, CDCl₃): δ = 10.72 (s, 1H), 8.53 (s, 1H), 8.33 (s, 1H), 7.94–7.88 (m, 4H), 7.57 (d, *J* = 5 Hz, 4H), 7.21 (d, *J* = 6.5 Hz, 4H), 4.46 (m, 4H), 4.30–4.27 (m, 6H), 2.65 (t, *J* = 7 Hz, 4H), 2.16–2.10 (m, 4H), 2.0–1.96 (m, 6H), 1.69 (m, 8H), 1.66–1.63 (m, 4H), 1.49–1.20 (m, 108 H), 0.88–0.83 ppm (m, 21H); ¹³C NMR (125 MHz, CDCl₃): δ = 149.83, 148.24, 147.63, 146.94, 143.89, 143.07, 142.98, 138.89, 138.11, 136.49, 131.58, 130.91, 129.40, 127.52, 125.69, 123.88, 123.33, 121.44, 119.27, 111.43, 106.86, 104.99, 104.40, 95.21, 86.64, 68.72, 68.54, 68.34, 68.08, 67.91, 35.04, 30.94, 30.30, 28.78, 28.73, 28.68, 28.65, 28.55, 28.41, 28.35, 28.12, 25.31, 25.27, 25.17, 21.69, 13.10 ppm; elemental analysis: C₁₂₀H₁₈₂N₂O₅; calculated (%): C

83.18, H 10.59, N 1.62; found: C 83.26, H 10.64, N 1.68. ^1H NMR and ^{13}C NMR spectra are shown in the ESI Fig. S6.

14b: IR (film) ν_{max} = 2924, 2893, 2852, 2208, 1606, 1510, 1454, 1377, 1249, 1163, 1078 cm^{-1} ; ^1H NMR (500 MHz, CDCl_3): δ = 10.70 (s, 1H), 8.47 (s, 1H), 8.24 (s, 1H), 7.86–7.83 (m, 4H), 7.58 (br, 4H), 6.90 (d, J = 8 Hz, 4H), 4.43 (m, 4H), 4.30–4.24 (m, 6H), 4.01 (t, J = 6.5 Hz, 4H), 2.16–2.11 (m, 4H), 2.09–1.97 (br, 6H), 1.82–1.79 (m, 4H), 1.69–1.21 (m, 94H), 1.01 (t, J = 7 Hz, 6H), 0.88 ppm (br, 15H); ^{13}C NMR (125 MHz, CDCl_3) = 159.78, 159.71, 151.64, 150.91, 149.40, 148.76, 148.07, 144.97, 140.10, 139.31, 137.61, 133.48, 133.45, 132.32, 131.57, 130.54, 127.24, 126.80, 126.68, 125, 124.47, 122.65, 118.08, 114.64, 112.62, 108.62, 105.69, 96.36, 96.21, 87.07, 69.85, 69.67, 69.49, 69.21, 69.02, 67.83, 31.96, 31.29, 29.82, 29.79, 29.75, 29.73, 29.66, 29.62, 29.57, 29.54, 29.42, 29.21, 26.31, 26.27, 26.20, 22.71, 19.26, 14.12, 13.87 ppm; elemental analysis: $\text{C}_{108}\text{H}_{158}\text{N}_2\text{O}_7$; calculated (%): C 81.25, H 9.98, N 1.75; found: C 81.34, H 10.05, N 1.84. ^1H NMR and ^{13}C NMR spectra are shown in the ESI, Fig. S7.

14c: IR (film) ν_{max} = 2956, 2924, 2852, 2206, 1606, 1510, 1454, 1377, 1249, 1163, 1078 cm^{-1} ; ^1H NMR (500 MHz, CDCl_3): δ = 10.68 (s, 1H), 8.44 (s, 1H), 8.20 (s, 1H), 7.84–7.81 (m, 4H), 7.58 (br, 4H), 6.90 (d, J = 8 Hz, 4H), 4.41 (br, 4H), 4.28–4.23 (m, 6H), 3.99 (t, J = 6 Hz, 4H), 2.16–2.10 (m, 4H), 1.97 (br, 6H), 1.82 (t, J = 6.5 Hz, 4H), 1.68–1.58 (m, 12H), 1.49–1.21 (m, 98H), 0.90–0.84 ppm (m, 21H); ^{13}C NMR (125 MHz, CDCl_3) = 158.65, 158.58, 150.16, 149.56, 148.03, 147.39, 146.66, 143.62, 138.57, 137.82, 136.09, 132.46, 132.41, 131.03, 130.47, 129.15, 125.67, 125.41, 125.20, 123.80, 123.69, 123.06, 121.26, 94.95, 94.88, 68.49, 68.36, 68.06, 67.92, 67.77, 67.10, 30.97, 30.84, 28.97, 28.84, 28.77, 28.68, 28.64, 28.44, 28.42, 28.30, 28.27, 28.16, 25.37, 25.34, 25.30, 25.15, 25.09, 25.07, 21.71, 21.67, 13.11 ppm; elemental analysis:

$C_{116}H_{174}N_2O_7$; calculated (%): C 81.54, H 10.26, N 1.64; found: C 81.74, H 10.41, N 1.79. 1H NMR and ^{13}C NMR spectra are shown in the ESI, Fig. S8.

14d: IR (film) ν_{max} = 2956, 2906, 2895, 2210, 1606, 1529, 1454, 1377, 1249, 1161, 1078 cm^{-1} ; 1H NMR (500 MHz, $CDCl_3$): δ = 10.76 (s, 1H), 8.52 (s, 1H), 8.34 (s, 1H), 7.97–7.90 (m, 4H), 7.57 (br, 4H), 6.90 (d, J = 8 Hz, 4H), 4.50–4.46 (m, 4H), 4.32–4.26 (m, 6H), 4.0 (t, J = 6.5 Hz, 4 H), 2.18–2.10 (m, 4H), 2.0–1.96 (m 6H), 1.81 (t, J = 6.5 Hz, 4H), 1.71–1.20 (m, 110H), 0.88–0.85 ppm (m, 21H); ^{13}C NMR (125 MHz, $CDCl_3$) = 158.66, 158.59, 151.22, 150.17, 149.59, 148.06, 147.42, 146.68, 143.63, 138.59, 138.21, 137.82, 136.10, 135.06, 132.46, 132.41, 131.01, 130.47, 129.69, 129.17, 127.81, 125.70, 125.44, 125.24, 123.82, 123.69, 123.09, 121.28, 116.54, 114.11, 113.54, 113.52, 113.04, 111.32, 106.51, 104.65, 104.14, 103.94, 94.99, 94.92, 86.17, 68.51, 68.39, 68.09, 67.94, 67.79, 67.11, 35.12, 33.30, 32.81, 30.97, 30.93, 29.29, 28.86, 28.84, 28.77, 28.71, 28.68, 28.67, 28.65, 28.52, 28.48, 28.46, 28.44, 28.37, 28.35, 28.32, 28.29, 28.23, 28.13, 25.37, 25.34, 25.30, 25.15, 25.10, 25.08, 21.71, 21.69, 13.11 ppm; elemental analysis: $C_{128}H_{198}N_2O_7$; calculated (%): C 81.91, H 10.63, N 1.49; found: C 82.29, H 10.74, N 1.83. 1H NMR and ^{13}C NMR spectra are shown in the ESI, Fig. S9.

14e: IR (film) ν_{max} = 2955, 2918, 2850, 2210, 1606, 1514, 1454, 1377, 1259, 1161, 1074 cm^{-1} ; 1H NMR (500 MHz, $CDCl_3$): δ = 10.71 (s, 1H), 8.47 (s, 1H), 8.25 (s, 1H), 7.88–7.84 (m, 4H), 7.57 (br, 4H), 6.90 (d, J = 7.5 Hz, 4H), 4.44 (br, 4H), 4.30–4.25 (m, 6H), 3.99 (t, J = 6 Hz, 4H), 2.17–2.09 (m, 4H), 1.98 (br, 6H), 1.83–1.80 (m, 4H), 1.69–1.58 (m, 14H), 1.48–1.21 (m, 136 H), 0.88–0.84 ppm (m, 21H); ^{13}C NMR (125 MHz, $CDCl_3$) = 159.72, 151.66, 150.93, 149.41, 148.78, 148.10, 144.99, 140.12, 139.33, 137.63, 133.48, 133.45, 132.32, 131.57, 130.56, 127.27, 126.82, 126.71, 125.01, 124.49, 122.67, 118.11, 114.98, 114.65, 108.10, 105.73, 105.57, 96.39, 87.10, 69.86, 69.69, 69.52, 69.23, 69.04, 68.18, 31.96, 29.79, 29.73, 29.68, 29.66, 29.63, 29.57,

29.54, 29.48, 29.46, 29.42, 29.38, 29.28, 29.27, 26.31, 26.28, 26.21, 26.08, 22.71, 14.12 ppm; elemental analysis: C₁₃₆H₂₁₄N₂O₇; calculated (%): C 82.12, H 10.84, N 1.41; found: C 82.19, H 10.91, N 1.52. ¹H NMR and ¹³C NMR spectra are shown in the ESI, Fig. S10.

14f: IR (film) ν_{\max} = 2949, 2924, 2852, 2210, 1606, 1512, 1454, 1377, 1261, 1161, 1080 cm⁻¹; ¹H NMR (500 MHz, CDCl₃): δ = 10.75 (s, 1H), 8.52 (s, 1H), 8.20 (s, 1H), 7.92 (m, 4H), 7.59–7.57 (m, 4H), 6.91 (d, *J* = 8.5 Hz, 4H), 4.48 (br, 4H), 4.32–4.27 (m, 6H), 4.03 (t, *J* = 6.5 Hz, 4H), 2.16–2.0 (m, 4H), 1.99–96 (m, 6H), 1.71–1.67 (m, 2H), 1.65–1.17 (m, 102H), 0.97 (d, *J* = 6.5 Hz, 6H), 0.89–0.83 ppm (m, 33H); ¹³C NMR (125 MHz, CDCl₃) = 159.76, 159.69, 151.58, 150.88, 149.35, 148.73, 148.04, 144.94, 140.06, 139.25, 137.54, 133.48, 133.45, 132.28, 131.58, 130.51, 127.19, 126.77, 126.65, 124.97, 124.44, 124.03, 123.49, 122.61, 118.02, 115.95, 115, 114.91, 114.65, 114.07, 112.57, 108, 106.19, 105.63, 105.45, 96.34, 96.20, 87.09, 69.82, 69.64, 69.45, 69.19, 69, 66.49, 39.27, 37.36, 37.34, 36.18, 31.96, 31.63, 29.92, 29.91, 29.83, 29.80, 29.78, 29.74, 29.71, 29.68, 29.64, 29.58, 29.55, 29.43, 29.13, 28.01, 26.32, 26.28, 26.20, 24.69, 22.72, 22.63, 19.68 ppm; elemental analysis: C₁₂₀H₁₈₂N₂O₇; calculated (%): C 81.67, H 10.40, N 1.59; found: C 82.05, H 10.72, N 1.81. ¹H NMR and ¹³C NMR spectra are shown in the ESI, Fig. S11.

7. Conclusions

A new class of triphenylene based discotic liquid crystals were synthesised using Sonogashira coupling reaction between alkoxy phenylene acetylene or alkyl phenylacetylene with intermediate dibrominated phenazine fused triphenylene. All the extended mesogens were self-assembled into hexagonal columnar mesophase over wide temperature range and retains liquid crystalline properties upto room temperature upon cooling from isotropic liquid. The liquid crystalline properties were investigated using polarised optical microscopy, differential scanning

calorimetry. The mesophase structure of all the mesogens were investigated using X-ray diffraction studies. All the extended discotic compounds exhibit strong photoluminescence properties in the anhydrous chloroform solvent. The π - extended heteroaromatic triphenylene discotic mesogens enhance nonlinear optical properties and are suitable for materials for electro-optical applications

Acknowledgments

The authors thank Dr. Vijayaragavan for recording NMR spectra, Dr. Srinivas HT and Ms. Vasuda for their technical support.

Supplementary information

The general methods, POM textures, DSC thermograms, TGA, XRD, NLO setup and spectral data have been given in supplementary information.

References

- [1] Li Q. Self-Organized Semiconductors: From Materials to Device Applications, John Wiley & Sons, New York, 2011.
- [2] Tovar JD. Supramolecular Construction of Optoelectronic Biomaterials. *Acc Chem Res* 2013;46:1527–1537.
- [3] Hoeben FJM, Jonkheijm P, Meijer EW, Schenning APHJ. About supramolecular assemblies of π -conjugated systems. *Chem Rev* 2005;105:1491–1546.
- [4] Kato T. Self-Assembly of Phase-Segregated Liquid Crystal Structures *Science* 2002;295:2414–2418.
- [5] Kato T, Mizoshita N, Kishimoto K. Functional Liquid-Crystalline Assemblies: Self-Organized Soft Materials. *Angew Chem Int Ed* 2006;45:38–68.

- [6] Chandrasekhar S, Sadashiva BK, Suresh KA. Liquid crystals of disc-like molecules. *Pramana* 1977;9:471–480.
- [7] Kumar S. Chemistry of discotic liquid crystals: from monomers to polymers, CRC Press, Boca Raton, FL, 2011
- [8] Kumar S. Self-organization of disc-like molecules: chemical aspects. *Chem Soc Rev* 2006;35:83–109.
- [9] Bisoyi HK, Kumar S. Discotic Nematic Liquid Crystals: Science and Technology. *Chem Soc Rev* 2010;39:264–285.
- [10] Sergeyev S, Pisula W, Geerts YH. Discotic Liquid Crystals: A New Generation of Organic Semiconductors. *Chem Soc Rev* 2007;36:1902–1929.
- [11] Schmidt-Mende L, Fechtenkötter A, Mullen K, Moons E, Friend RH, MacKenzie JD. Self-Organized Discotic Liquid Crystals for High-Efficiency Organic Photovoltaics. *Science* 2001;293:1119–1122.
- [12] van de Craats AM, Stutzmann N, Bunk O, Nielsen MM, Watson M, Mullen K, Chanzy HD, Sirringhaus H, Friend RH. Meso-Epitaxial Solution-Growth of Self-Organizing Discotic Liquid-Crystalline Semiconductors. *Adv Mater* 2003;15:495–499.
- [13] Schmidtke JP, Friend RH, Kastler M, Mullen K. Control of morphology in efficient photovoltaic diodes from discotic liquid crystals. *J Chem Phys* 2006;124:174704.
- [14] Kaafarani BR. Discotic Liquid Crystals for Opto-Electronic Applications. *Chem Mater* 2010;23:378–396.

- [15] Boden N, Bushby RJ, Clements J, Movaghar B. Device applications of charge transport in discotic liquid crystals. *J Mater Chem* 1999;9:2081–2086.
- [16] Bushby RJ, Kawata K. Liquid Crystals that Affected the World: Discotic Liquid Crystals. *Liq Cryst* 2011;38:1415–1426.
- [17] van de Craats AM, Warman JM. The Core-Size Effect on the Mobility of Charge in Discotic Liquid Crystalline Materials. *Adv Mater* 2001;13:130–133.
- [18] Ye Q, Chang J, Shao J, Chi C. Large Core-Expanded Triazatruxene-Based Discotic Liquid Crystals: Synthesis, Characterization and Physical Properties. *J Mater Chem* 2012;22:13180–13186.
- [19] Kumar S, Varshney SK. A Room-Temperature Discotic Nematic Liquid Crystal. *Angew Chem Int Ed* 2000;39:3140–3142.
- [20] Goodby J, Collings PJ, Kato T, Tschierske C, Gleeson HF, Raynes P.eds. *Handbook of Liquid Crystals, Vol. 4, part III*, p. 467, Wiley-VCH, Weinheim, Germany, 2014.
- [21] Kumar M, Gowda A, Kumar S. Discotic Liquid Crystals with Graphene: Supramolecular Self-assembly to Applications. *Part Part Syst Charact* 2017;34:1700003.
- [22] Gowda A, Kumar M, Kumar S. Discotic liquid crystals derived from polycyclic aromatic cores: from the smallest benzene to the utmost graphene cores. *Liq Cryst* 2017;44:1990–2017.
- [23] Nair GG, Rao DSS, Prasad SK, Chandrasekhar S, Kumar S. Electrooptic and Viewing Angle Characteristics of a Display Device Employing a Discotic Nematic Liquid Crystal. *Mol Cryst Liq Cryst* 2003;397:245–252.

- [24] Kumar S, Varshney SK. Design and Synthesis of Discotic Nematic Liquid Crystals. *Org. Lett* 2002;4:157–159.
- [25] Kumar S. Molecular engineering of discotic nematic liquid crystals. *Pramana* 2003;61:199–203.
- [26] Mori H, Itoh Y, Nishuira Y, Nakamura T, Shinagawa Y. Performance of a Novel Optical Compensation Film Based on Negative Birefringence of Discotic Compound for Wide-Viewing-Angle Twisted-Nematic Liquid-Crystal Displays. *Jpn J Appl Phys* 1997;36:143–147.
- [27] Kawata K. Orientation Control and Fixation of Discotic Liquid Crystal. *Chem Rec* 2002;2:59–80.
- [28] Cammidge AN, Gopee H. In *Handbook of Liquid Crystals*, 2nd ed.; Goodby, J. W., Collings, P. J., Kato, T., Tschierske, C., Gleeson, H. F., Raynes, P., Eds.; Vol. 3, pp 293–334, Wiley-VCH Verlag GmbH: Weinheim, 2014
- [29] van de Craats AM, Warman JM, Fechtenkötter A, Brand JD, Harbison MA, Müllen K. Record Charge Carrier Mobility in a Room Temperature Discotic Liquid-Crystalline Derivative of Hexabenzocoronene. *Adv Mater* 1999;11:1469–1472.
- [30] Shklyarevskiy IO, Jonkheijm P, Stutzmann N, Wasserberg D, Wondergem HJ, Christianen PCM, Schenning A, de Leeuw DM, Tomovic Z, Wu JS, Müllen K, Maan JC. High Anisotropy of the Field-Effect Transistor Mobility in Magnetically Aligned Discotic Liquid-Crystalline Semiconductors. *J Am Chem Soc* 2005;127:16233–16237.
- [31] Tracz A, Jezka JK, Watson MD, Pisula W, Müllen K, Pakula T. Uniaxial Alignment of the Columnar Super-Structure of a Hexa (Alkyl) Hexa-peri-

- hexabenzocoronene on Untreated Glass by Simple Solution Processing. *J Am Chem Soc* 2003;125:1682–1683.
- [32] Pisula W, Tomovic Z, El Hamaoui B, Watson MD, Pakula T, Müllen K. Control of the Homeotropic Order of Discotic Hexa-*peri*-hexabenzocoronenes. *Adv Funct Mater* 2005;15:893–904.
- [33] Balagurusamy VSK, Prasad SK, Chandrasekhar S, Kumar S, Manickam M, Yelamaggad CV. Quasi-one dimensional electrical conductivity and thermoelectric power studies on a discotic liquid crystal. *Pramana* 1999;53:3–11.
- [34] Iino H, Hanna J, Bushby RJ, Movaghar B, Whitaker BJ, Cook MJ. Very high time-of-flight mobility in the columnar phases of a discotic liquid crystal. *Appl Phys Lett* 2005;87:132102.
- [35] Bunk O, Nielsen MM, Solling TI, van de Craats AM, Stutzmann N. Induced Alignment of a Solution-Cast Discotic Hexabenzocoronene Derivative for Electronic Devices Investigated by Surface X-ray Diffraction. *J Am Chem Soc* 2003;125:2252–2258.
- [36] Boden N, Bushby RJ, Cammidge AN, Clements J, Luo R, Donovan KJ. Transient Photoconductivity and Dark Conductivity in Discotic Liquid Crystals. *Mol Cryst liq Cryst* 1995;261:251–257.
- [37] Bacher A, Bleyl I, Erdelen CH, Haarer D, Paulus W, Schmidt HW. Low molecular weight and polymeric triphenylenes as hole transport materials in organic two-layer LEDs. *Adv Mater* 1997;9:1031–1035.

- [38] Seguy I, Jolinat P, Destruel P, Farenc J, Mamy R, Bock H, Ip J, Nguyen TP. Red organic light emitting device made from triphenylene hexaester and perylene tetraester. *J Appl Phys* 2001;89:5442–5448.
- [39] Hassheider T, Benning SA, Kitzerow HS, Achardand MF, Bock H. Color-Tuned Electroluminescence from Columnar Liquid Crystalline Alkyl Arenecarboxylates. *Angew Chem Int Ed* 2001;40:2060–2063.
- [40] Cherian S, Donley C, Mathine D, LaRussa L, Xia W, Armstro N. Effects of field dependent mobility and contact barriers on liquid crystalline phthalocyanine organic transistors. *J Appl Phys* 2004;96:5638–5643.
- [41] Xiao S, Myers M, Miao Q, Sanaur S, Pang K, Steigerwald ML, Nuckolls C. Molecular Wires from Contorted Aromatic Compounds. *Angew Chem Int Ed* 2005;44:7390–7394.
- [42] Cho J.-Y, Domercq B, Jones SC, Yu J, Zhang X, An Z, Bishop M, Barlow S, Marder SR, Kippelen B. High electron mobility in nickel bis(dithiolene) complexes. *J Mater Chem* 2007;17:2642–2647.
- [43] Adam D, Schuhmacher P, Simmerer J, Haussling L, Selemensmeyer K, Etbach KH, Ringsdorf H, Haarer D. Fast photoconduction in the highly ordered columnar phase of a discotic liquid crystal. *Nature* 1994;371:141–143.
- [44] Kumar M, Kumar S. Liquid crystals in photovoltaics: a new generation of organic photovoltaics. *Nature Poly J* 2017;49:85–111.
- [45] Clements J, Boden N, Gibson TD, Chandler RC, Hulbert JN, Ruck-Keene EA. Novel, self-organising materials for use in gas sensor arrays: beating the humidity problem. *Sens Actuators B* 1998;47:37–42.

- [46] Wright JD, Roisin P, Rigby GP, Nolte RJM, Cook MJ, Thorpe SC. Crowned and liquid-crystalline phthalocyanines as gas-sensor materials. *Sens Actuators E* 1993;13:276–280.
- [47] Kumar S. Recent developments in the chemistry of triphenylene-based discotic liquid crystals. *Liq Cryst* 2004;31:1037–1059.
- [48] Kumar S. Triphenylene-based discotic liquid crystal dimers, oligomers and polymers. *Liq Cryst* 2005;32:1089–1113.
- [49] Laschat S, Baro A, Steinke N, Giesselmann F, Hgele C, Scalia G, Judele R, Kapatsina E, Sauer S, Schreivogel A, Tosoni M. Discotic Liquid Crystals: From Tailor-Made Synthesis to Plastic Electronics. *Angew Chem Int Ed* 2007;46:4832 – 4887.
- [50] Pal SK, Setia S, Avinash BS, Kumar S. Triphenylene-based discotic liquid crystals: recent advances. *Liq Cryst* 2013;40:1769–1816.
- [51] Wohrle T, Wurzbach I, Kirres J, Kostidou A, Kapernaum N, Litterscheidt J, Haenle JC, Staffeld P, Baro A, Giesselmann F, Laschat S. Discotic Liquid Crystals. *Chem Rev* 2016;116:1139–1241.
- [52] Feng X, Marcon V, Pisula W, Hansen MR, Kirkpatrick J, Grozema F, Andrienko D, Kremer K, Müllen k. Towards high charge-carrier mobilities by rational design of the shape and periphery of discotics. *Nat Mater* 2009;8:421–426.
- [53] van de Craats AM, Warman JM, de Haas MR, Adam D, Simmerer J, Haarer D, Schuhmacher P. The Mobility of Charge Carriers in All Four Phases of the Columnar Discotic Material Hexakis(hexylthio)triphenylene: Combined TOF and PR-TRMC Results. *Adv Mater* 1996;8:823–826.

- [54] Kumar S, Manickam M. Synthesis of phenanthro[a] phenazine derivatives: a novel ring structure forming discotic liquid crystals. *Liq Cryst* 1999;26:1097–1099.
- [55] Kumar S, Manickam M. Synthesis of phenanthro[b] phenazine, a novel heterocyclic ring structure for discotic liquid crystals. *Mol Cryst Liq Cryst* 2000;338:175–179.
- [56] Yatabe T, Harbison MA, Brand JD, Wagner M, Mullen K, Samori P, Rabe JP. Extended triphenylenes: synthesis, mesomorphic properties and molecularly resolved scanning tunneling microscopy images of hexakis(dialkoxyphenyl)triphenylenes and dodeca(alkoxy)tris(triphenylenylene)s. *J Mater Chem* 2000;10:1519–1525.
- [57] Cammidge AN, Gopee H. Macrodiscotic triphenylenophthalocyanines. *Chem Commun* 2002;966–967.
- [58] Kong X, He Z, Zhang Y, Mu L, Liang C, Chen B, Jing X, Cammidge AN. A Mesogenic Triphenylene–Perylene–Triphenylene Triad. *Org Lett* 2015;13:764–767.
- [59] Zhao B, Liu B, Png RQ, Zhang K, Lim KA, Luo J, Shao J, Ho PKH, Chi C, Wu J. New Discotic Mesogens Based on Triphenylene-Fused Triazatruxenes: Synthesis, Physical Properties, and Self-Assembly. *Chem Mater* 2010;22:435–449.
- [60] Kumar S, Gupta SK. Novel triphenylenoimidazole discotic liquid crystals. *Tetrahedron Lett* 2011;52:5363–5367.
- [61] Gowda A, Jacob L, Singh DP, Douali R, Kumar S. Charge Transport in Novel Phenazine Fused Triphenylene Supramolecular Systems. *ChemistrySelect* 2018;3:6551–6560.
- [62] Kumar S, Manickam M. Synthesis of Functionalized Triphenylenes by Selective Ether Cleavage with *B*-Bromocatecholborane. *Synthesis* 1998;8:1119–1122.

- [63] Kumar S, Manickam M, Varshney SK, Rao DSS, Prasad SK. Novel heptasubstituted triphenylene discotic liquid crystals. *J Mater Chem* 2000;10:2483–2489.
- [64] Shao J, Chang J, Chi C. Linear and star-shaped pyrazine-containing acene dicarboximides with high electron-affinity. *Org Biomol Chem* 2012;10:7045–7052.
- [65] Arakawa Y, Nakajima S, Ishige R, Uchimura M, Kang S, Konishi G.-I, Watanabe J. Synthesis of diphenyl-diacetylene-based nematic liquid crystals and their high birefringence properties. *J Mater Chem* 2012;22:8394–8398.
- [66] Gowda A, Jacob L, Joy N, Philip R, Rao P, Kumar S. *New J Chem* 2018;42:2047–2057.
- [67] R.L. Sutherland with contributions by D.G. McLean and S. Kirkpatrick, *Handbook of Nonlinear Optics*, second ed. New York, NY: Marcel Dekker, 2003.
- [68] Philip R, Kumar GR, Sandhyarani N, Pradeep T. Picosecond optical nonlinearity in monolayer-protected gold, silver, and gold-silver alloy nanoclusters. *Phys Rev B* 2000;62:13160.
- [69] Bredas JL, Adant C, Tackx P, Persoons A, Pierce BM. Third-Order Nonlinear Optical Response in Organic Materials: Theoretical and Experimental Aspects. *Chem Rev* 1994;94:243–278.